AIAA JOURNAL
Vol. 35, No. 2, February 1997

Panel-Structure Response to Acoustic Forcing by a Nearly Sonic Jet

C. C. Fenno Jr.*
National Research Council, Hampton, Virginia 23681-0001
A. Bayliss†
Northwestern University, Evanston, Illinois 60208
and
L. Maestrello‡
NASA Langley Research Center, Hampton, Virginia 23681-0001

A model of a high subsonic jet with a nearby array of flexible, aircraft-type panels is studied numerically in two dimensions. The jet is excited by a limited duration, spatially localized starter pulse in the potential core. The long time evolution of unsteady disturbances in the jet, the responses of the panels, and the ensuing radiation are computed and compared with those of a lower Mach number jet. The results show that, for high subsonic Mach numbers, the spectral response of both the jet (near and far field) and of the panels is concentrated in a relatively narrow frequency band centered at a Strouhal number (based on jet exit velocity) of approximately 0.25 and associated harmonics. This behavior of the jet and the panels is caused by nearly periodic vortex shedding from the nozzle lip. In contrast, for lower Mach numbers vortex shedding is very much weaker and the panels act as narrow-band filters emphasizing the natural frequencies of the panels. Radiation from the panels is weakest in upstream directions and exhibits zones of silence due to destructive interference of radiation from the different panels.

I. Introduction

THIS paper describes the results of a numerical simulation of jet noise in the presence of four flexible aircraft-type panels in a panel-stringer assembly. The simulation is based on a model that fully couples the fluid dynamics of the jet flow to the panel motion and the resulting acoustic radiation. The primary objective is to determine the role played by near sonic jet exit conditions on installation effects (i.e., the mounting of the jet near a flexible structure) and on the response and the acoustic radiation from the structure.

The long time evolution of unsteady disturbances in a nearly sonic jet exiting from a converging nozzle, together with panel responses and ensuing radiation from the panels, is considered in this paper. In previous work, jet acoustics, panel response, and radiation have been considered for lower-speed jets exiting from straight pipes, both at rest[1] and in forward motion.[2] The present results show qualitatively different behavior for high subsonic jets, namely, a relatively narrow-band jet and panel response concentrated at a Strouhal number of approximately 0.25. The mechanism driving this behavior is vortex shedding from the nozzle lip, which dominates jet and panel behavior for high subsonic Mach number jets. In contrast, for lower Mach number jets as considered in Ref. 1, there is a low-frequency jet response without pronounced spectral peaks. In this case the panels act as narrow-band filters converting the relatively broadband incident pressure into selected low-frequency bands associated with the natural frequencies of the panels, whereas the vortex shedding frequency is considerably less evident.

In previous analyses, the exact sources of jet noise have been identified from the basic equations of fluid dynamics.[3–6] Generally, these exact sources must be modeled in some way for computation. An important feature of the present method is the direct computation of at least some of the natural sources of jet noise, namely, fluid dynamical instability waves that develop due to instability of the jet shear layer. Experiments have demonstrated the existence of large-scale structures or instability waves in jets.[7–9] These structures are believed to act as sources of sound, a point also confirmed by analytical studies[10–13] and computations.[9,14,15]

The geometry of the computational model is shown in Fig. 1. The Euler equations are solved in two domains: the jet domain and the radiation domain separated by an array of four flexible panels. Panel response and radiation are also computed and are fully coupled to the fluid dynamics in the sense that at each time step the fluid dynamics (Euler) computation provides the pressure difference across the panels, thereby allowing computation of panel displacement and velocity. The resulting panel velocity then serves as a boundary condition for the Euler computation. Thus, no modeling of the panel excitation is needed. Other approaches to the general problem of describing panel loadings are possible, e.g., Ref. 16. Similar computations for boundary layers and for panels excited by large-amplitude acoustic disturbances in an ambient medium have also been performed.[17,18]

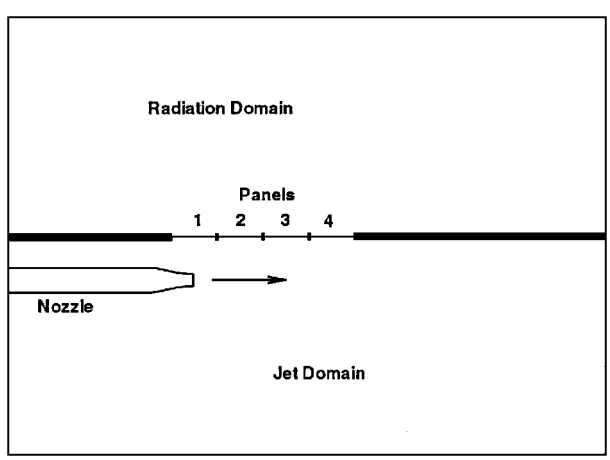

Fig. 1 Computational domain.

Received Feb. 3, 1996; revision received Aug. 27, 1996; accepted for publication Sept. 4, 1996; also published in *AIAA Journal on Disc*, Volume 2, Number 1.

*National Research Council Resident Research Associate, Fluid Mechanics and Acoustics Division, Mail Stop 463, NASA Langley Research Center. Member AIAA.

†Professor, Department of Engineering Sciences and Applied Mathematics.

‡Senior Research Scientist, Fluid Mechanics and Acoustics Division, Mail Stop 463. Associate Fellow AIAA.

The paper is organized as follows. In the next section there is a description of the model and a discussion of the numerical method and boundary conditions. In Sec. III, results are presented, first for the case of a free jet, then for the full jet flow/acoustic/structural interaction, and finally, the jet and panel responses are compared with those for a lower Mach number jet. The results are summarized and conclusions are drawn in Sec. IV.

II. Numerical Method

The computational domain is shown in Fig. 1. Unsteady pressure, density, and velocity are computed in two regions. The lower domain in Fig. 1 contains the jet, exiting from a contracting nozzle of width D, whereas in the upper domain (modeling the aircraft interior) only disturbances due to the panel radiation are present. These two regions will be referred to as the jet and radiation domains, respectively. The wall boundary is a rigid wall containing four adjacent flexible panels (denoted as panels 1–4 in Fig. 1) with rigidly clamped boundaries, closely approximating current airframe construction. The panels vibrate in response to excitation by sound from the jet, thereby radiating acoustic disturbances into both domains. In the jet domain, the panel radiation level is significantly smaller than the acoustic disturbances generated by the jet. In the radiation domain, however, panel radiation is the sole source of acoustic disturbances.

The numerical method involves coupling the computation of a nonlinear equation governing the panel responses (the beam equation) to an Euler computation performed in both the jet and radiation domains. The panel vibration is fully coupled to the fluid dynamics in that at each time step the pressure difference across the panels, computed from the Euler computations, serves as a forcing term for the beam equation. Similarly, the displacement obtained from the beam equation is differentiated in time and is imposed as a boundary condition for the Euler computations. The numerical method has been described in detail in Ref. 1. Thus, the presentation here will be brief.

The nonlinear beam equation is

$$D_b \frac{\partial^4 z}{\partial x^4} - N_x(z)\frac{\partial^2 z}{\partial x^2} + \rho_b h \frac{\partial^2 z}{\partial t^2} + \gamma \frac{\partial z}{\partial t} = p^+ - p^- \qquad (1)$$

where z represents the beam transverse deflection, ρ_b is the mass per unit volume of the beam, h is the beam thickness, γ is the physical damping, $D_b = Mh^3/12(1 - \nu^2)$ is the bending stiffness of the beam, M is the modulus of elasticity, and ν is the Poisson ratio of the beam material. The coefficient of the nonlinear term $N_x(z)$ represents the tension created by the stretching of the plate due to bending. The pressures in the radiation and jet domains are p^+ and $p-$, respectively. The solution of Eq. (1) is obtained at each time step using an implicit finite difference method. The panels are assumed clamped at both ends.

The coupling of the beam computation to the Euler computation occurs through the forcing term given on the right-hand side of Eq. (1). The pressures p^+ and $p-$ are obtained from the Euler computation using an explicit scheme. The displacement at the new time level is then obtained from solving Eq. (1) one time step. The normal velocity v is then obtained from differentiating z and employed as a boundary condition to complete the update to the Euler computation. Since this procedure is employed at each time step, the fluid and structural calculations are fully coupled.

The Euler equations are solved in conservation form for the vector $\hat{\boldsymbol{w}}$, where

$$\hat{\boldsymbol{w}} = (\rho, \rho u, \rho v, E)^T$$

and where ρ is the density, u and v, are the x and y components of the velocity, respectively, and E is the total energy per unit volume,

$$E = \tfrac{1}{2}\rho(u^2 + v^2) + c_v \rho \tilde{T}$$

where $\tilde{T}$ is the temperature and c_v is the specific heat per unit volume. The pressure p is obtained from the equation of state. The Euler equations are solved separately in both the jet and radiation domains.

In the jet domain the Euler equations are modified to account for the jet flow. The jet exits from a nozzle of width D and the solution is computed both within and exterior to the nozzle. The Euler equations are modified to account for two different nonhomogeneous forcing terms.[1] One term serves as a starter pulse to excite the jet. It corresponds to a localized source of mass injection at the location (x_s, y_j), where y_j is the location of the jet axis ($3.5D$ from the wall) and x_s is approximately $1.15D$. An alternative approach, involving time harmonic excitation of the jet, is described in Ref. 19. The second forcing term is designed so that in the absence of the starter pulse the solution to the Euler equations would be a stationary profile corresponding to a spreading jet. The inclusion of this term separates the computation of the disturbance, in particular the resulting instability waves, from the computation of the mean flow (i.e., the spreading jet). Thus, the resulting system of equations allows for the simulation of instability waves and the resulting sound generation, together with the curving of acoustic waves in the jet flowfield, without requiring the computation of the spreading jet itself. Although this is a simplified model, it captures many of the observed features of instability wave generated jet sound and permits high-resolution computation of the coupling of jet noise with the flexible panels and the resulting radiation from the panels. In particular, the model allows for computation of the natural sources of jet noise (the instability waves) together with the sound radiated by these sources.

The initial conditions are taken to be ambient data in the radiation domain and the mean state in the jet domain. The model for the mean axial and normal velocities is obtained from Ref. 20 in Cartesian coordinates. The effect of the wall on the spreading of the jet is not considered in our model. In contrast to previous calculations[1,2] at lower jet speeds, the current study requires a mean flow model that addresses the compressibility of the flow. Thus, the mean pressure and density are also modeled. Inside the nozzle, the quasi-one-dimensional equations of isentropic flow are employed for pressure and temperature. Outside the nozzle, the jet pressure is obtained from Ref. 21. Centerline temperature is modeled assuming a constant total temperature and off-centerline temperature variations follow the axial velocity relaxation. Density follows from the state equation both inside and outside the nozzle. It is imperative that the mean flow be smooth up to and including its second derivative for the numerical simulation of instability flows.[22,23] Therefore, great care was taken in modeling the mean flow.

The boundary conditions are as follows (refer to Fig. 1).

1) Bounding wall—rigid conditions imposed except for the flexible panels, which are treated as described earlier.

2) Nozzle exterior—impedance boundary conditions used on the exterior of the nozzle, simulating the use of an absorbing material to absorb waves incident on the nozzle from the exterior.

3) Nozzle interior—rigid conditions used for the terminal two-thirds of the nozzle. The first third (near the inflow boundary) employs impedance conditions to reduce the possibility of reflections from the nozzle inflow.

4) Inflow for the nozzle—characteristic conditions. Specifically, the Euler equations are linearized about the ambient state, assumed to hold far upstream in the nozzle, and the three incoming characteristics

$$p + \rho c u, \qquad v, \qquad c_\infty \rho - p/c_\infty$$

are imposed to be the values that they would have far upstream. It has been shown that this boundary condition is valid for the lowest propagating mode in the nozzle.[9]

5) All other boundaries in the problem are artificial. Nonreflecting (radiation) boundary conditions are imposed to prevent spurious reflections from propagating into the interior. These boundary conditions are based on a far-field expansion of the solution.[24,25]

A finite difference scheme is employed that is fourth order accurate in space and second order in time. The scheme is a generalization of the second-order MacCormack scheme to allow higher-order accuracy in space.[26] The scheme has been discussed in detail.[9,15]

III. Results

The results are presented in three subsections: 1) simulation of a jet without a nearby structure (i.e., free jet), 2) the jet with the nearby structure, and 3) comparison between high subsonic and low Mach number jet. For the high subsonic jet, the jet exit Mach number is $M_j = 0.9$, whereas for the lower Mach number jet, $M_j = 0.65$. In each case the surrounding fluid is at rest. The nozzle utilizes a

converging geometry with a contraction ratio of 2:1 over a longitudinal distance of four exit widths. Figure 1 shows a sketch of the computational domain for the case, which includes the structure.

The grids used in this study utilize stretching to enhance resolution in y of the shear layer and resolution in x near the nozzle exit. The y grid is mapped to conform to the contracting nozzle, whereas the x grid remains Cartesian. This deviates slightly from orthogonality in the vicinity of the nozzle contraction but returns to a standard stretched Cartesian grid in all other regions. The computations have been extensively validated by grid refinement,[1,2] and, equally important, there are no spurious boundary reflections visible for the time interval considered in this paper ($tc_\infty / D \leq 100$).

A. Free Jet Results

For this case, nonreflecting boundary conditions are imposed on the upper boundary and the jet is centered in y. The origin of the x coordinate is at the nozzle exit. The domain extends $45D$ downstream, $30D$ upstream, and $30D$ in both directions normal to the jet axis. The computed solution is symmetric around the jet axis to a close approximation, although symmetry is not imposed in the computation. A grid with 581 points in the x direction and 901 points in the y direction is employed. Grid clustering is used in both dimensions to enhance resolution in the jet exit region.

The structure of the pressure and vorticity field near the nozzle exit are considered first. Shown in Fig. 2 are contours of the instantaneous vorticity and pressure fluctuation,

$$\tilde{p}(x, y, t) = p(x, y, t) - \bar{p}(x, y)$$

where $\bar{p}$ denotes the mean pressure, for a small region near the nozzle exit at $tc_\infty / D = 100$. The sources simulated by the model are vorticity disturbances shed from the nozzle lip due to the near discontinuity

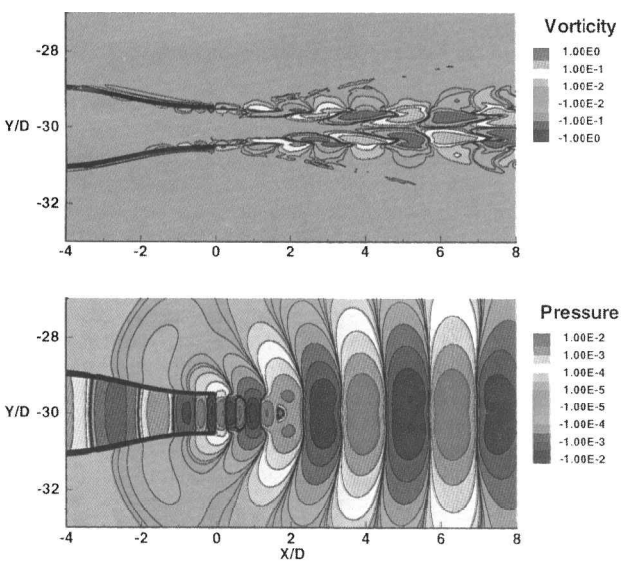

Fig. 2 Near-field vorticity and pressure contours.

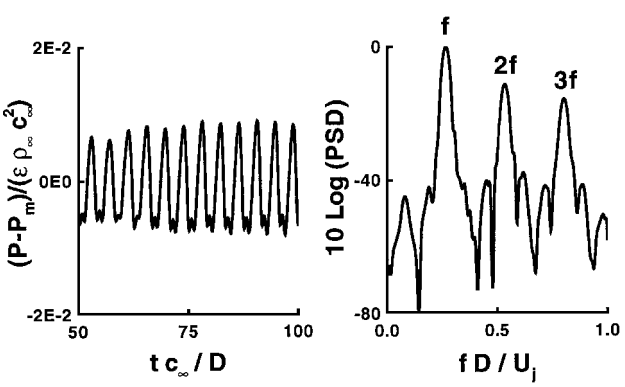

Fig. 3 Jet flowfield time history and spectrum at $x/D = 10$ and $(y - y_{axis})/D = 0.8$.

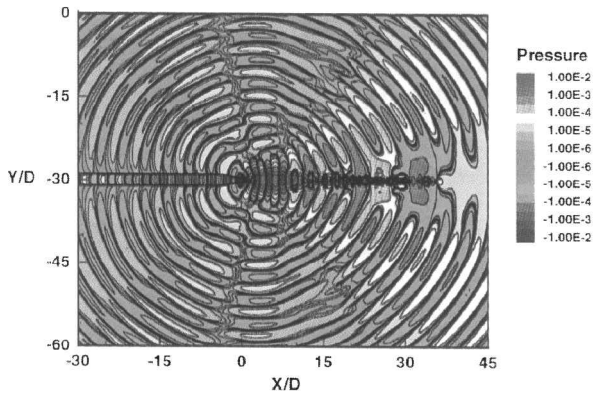

Fig. 4 Contours of $\tilde{p}$ for free jet.

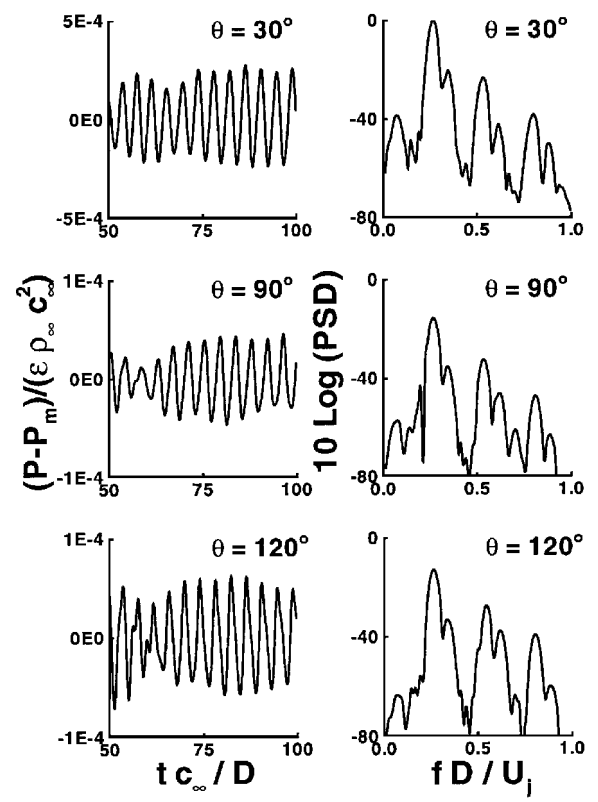

Fig. 5 Jet far-field time history and spectra at $\theta = 30$, 90, and 120 deg from the jet axis.

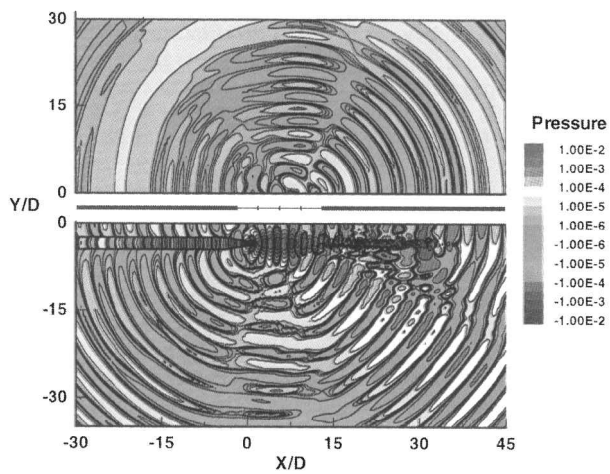

Fig. 6 Contours of $\tilde{p}$ in jet and radiation domains.

in the velocity profile at the lip. The shedding is nearly periodic and the vortices convect primarily downstream. As they propagate, pressure disturbances associated with the vortices travel both upstream and downstream, ultimately leading to far-field sound. The effect of the flowfield inside the nozzle on the wavelength of the upstream propagating disturbances can be seen from the shorter wavelengths due to the slower upstream wave speed in the contracted section.

Figure 3 shows the time history and spectrum of the fluctuating pressure $\tilde{p}$ at a point inside the jet flowfield ($x = 10D$ and $y - y_{\text{axis}} = 0.8D$). The power spectral density (PSD) is normalized to 0 dB based on the maximum of the spectra. Figure 3 shows that the spectral structure of the flowfield $\tilde{p}$ is composed of a fundamental frequency $f*$ such that the Strouhal number $S_r* = f*D/U_j \simeq 0.25$ where U_j is the jet exit velocity. The spectrum also shows two harmonics and one quarter subharmonic. This fundamental Strouhal number is close to observations of peak jet output (e.g., Ref. 27). The precise value of S_r* is certainly a property of the particular model used in the computations. However, this scaling for the shedding frequency has been confirmed for the model by computations with different jet Mach numbers in a limited range around 0.9 and with different jet widths. Examination of $\tilde{p}$ over an earlier time window indicates a more broadband structure due to sound generated from the leading instability wave generated from the starter pulse. The predominant long time feature of the excited jet predicted by the model is the nearly periodic shedding of vorticity from the nozzle lip. Computations with lower-speed jets (not shown) indicate that this behavior becomes much more pronounced as the jet approaches a sonic exit velocity.

The unsteady flowfield in the jet generates acoustic disturbances, which propagate into the far field as sound. Figure 4 shows a representation of $\tilde{p}$ over the entire computational domain at $tc_\infty/D = 100$. Although the flow is initially excited by a starter pulse, at the time for Fig. 4 this initial disturbance has propagated through and exited the computational domain. The remaining disturbances are generated due to instabilities of the jet shear layer. These disturbances convect downstream and spread with the jet. Analogous structures have been previously observed and computed in axisymmetric models.[7,9] Figure 4 also shows a series of waves propagating upstream into the far field together with a similar series of waves propagating downstream into the far field. The waves appear to be nearly periodic and are of similar spatial extent. Furthermore, they have the same frequency and wavelength. These waves are due to the nearly periodic shedding of vorticity from the nozzle lip (see Fig. 2) and the subsequent generation of pressure disturbances both inside and outside the jet. It can be seen from Fig. 4 that the upstream propagating waves appear to emanate from a point closer to the nozzle exit than the downstream propagating waves and also appear to be out of phase with the downstream propagating waves. This results in a region of interference between these two wave patterns along a ray directed approximately 100 deg from the jet axis.

There is also a wave pattern within the contracting nozzle. The fluid field within the nozzle is nearly constant in y, leading to a pattern of nearly plane waves. The boundary condition inside the nozzle is rigid up to $x = -10D$ and then is gradually changed to an absorbing boundary condition to help eliminate reflections from the inflow boundary. Animation of these data indicates that only upstream propagating waves are present in the nozzle.

The far-field pressure fluctuation is plotted in Fig. 5 as a function of tc_∞/D at three far-field angles ($\theta = 30$, 90, and 120 deg) taken on a circle of radius $20D$. At all three points selected, $\tilde{p}$ oscillates with a nearly constant period with a gradually varying amplitude. The period is close to that of the vorticity generation from the nozzle lip. Thus, the frequency is transmitted to the far field as sound.

In addition to the time history, the PSD of $\tilde{p}$ is shown in Fig. 5. The PSD is normalized to 0 dB based on the maximum of the spectra over the three angles. The figure shows that the far-field spectral structure is similar to the jet flowfield spectra (Fig. 3). The fundamental frequency corresponds to $S_r* \simeq 0.25$, and the two harmonics and one-quarter subharmonic are exhibited as in the jet flow. The amplitude of the first and second harmonics is increased, relative to the fundamental, if the amplitude of the starter pulse is increased, confirming that these harmonics are generated via nonlinear interactions. Furthermore, the presence of low-level subharmonics in the pressure spectra, again indicative of weak nonlinearities, is seen. Finally, it is seen that the spectra reach a maximum at $\theta \simeq 30$ deg, consistent with experiments and previous computations.[2,8,9] This preferred direction is independent of the presence of the wall. The relative harmonic content of the time signal increases as θ increases. Thus there is a preferred upstream directivity for high frequencies (i.e., the harmonics).

B. Jet/Structure Interaction

Referring again to Fig. 1, a wall, assumed infinite in extent and parallel to the nozzle, is located $3.5D$ above the jet. The wall is assumed rigid, except for four flexible, aircraft-type panels with clamped boundaries. Each of the panels is of length $3.5D$ and thickness $0.01D$. The panels are centered at $x/D = 0$, 3.75, 7.50, and 11.25, respectively. These are referred to as panels 1, 2, 3, and 4. Characteristic parameters of the panels are typical of aluminum.

The grid in the jet domain is comparable to that described earlier for the free jet. To allow a greater distance between the jet and the artificial lower boundary the y domain extends down $45D$. The panels are at the origin in the vertical direction. The Euler equations are also solved in the radiation domain. Using the fully coupled model, we computed the unsteady disturbances in the jet, which serve to excite the panels, the responses of the panels, and the radiation from the panels into both the jet domain and the radiation domain.

A contour plot of the unsteady flow and acoustic field can be seen in Fig. 6. In the jet domain the large-scale structure propagating downstream is observed, trailed by other pressure disturbances in the jet. The generation of disturbances from the nozzle lip is clearly visible and occurs on a continual basis as time evolves. There is a series of ripples corresponding to acoustic disturbances that radiate into the far field. The upstream radiation again appears to emanate from sources close to the nozzle exit, whereas the downstream radiation emanates from sources further downstream, resulting in an interference pattern in the range $80 \lesssim \theta \lesssim 100$ deg. The waves radiated downstream have higher amplitudes, and the peak radiation occurs at around 30 deg.

A series of outwardly propagating ripples, representing acoustic radiation from the panels, can be seen in the radiation domain. Since these ripples emanate from all four panels, it is not possible to ascribe a precise geometric origin to them. Thus, instead of angles, far-field locations in the radiation domain are designated by x/D values along a line at $y/D = 25$. The wavelength is comparable to the wavelength of the downstream radiated sound in the jet; i.e., the wavelength and frequency are controlled by S_r*. The wave pattern in the radiation domain is more sharply defined than that observed in Ref. 1 for a lower Mach number jet. Those results concentrated on earlier times and lower-speed jets than the present computation. The largest overall level of sound radiation occurs at roughly 90 deg and the level is larger in downstream directions than in upstream directions. Details of these radiation levels are discussed in Sec. III.B.3.

Features of the fully coupled flow/acoustics/structural flowfield are described next. The jet domain, panel responses, and radiation domain are examined.

1. *Jet Flow Domain*

In Fig. 7 the far-field directivity is shown for both the free jet and the jet in the presence of a nearby wall. The data are given along an arc $20D$ from the jet exit and for angles below the centerline. Far-field pressures with the wall are similar to those described previously for the jet without any wall. Over the time interval considered, the differences are of the order of 5 dB. Note that one would expect differences on the order of 3 dB in power from a rigid infinite surface at normal incidence. Since there are distributed sources and the surface itself is flexible, these differences are not surprising.

In Fig. 8, the incident pressure at the center of the panels is shown in both the time and frequency domains. The overall level of $\tilde{p}$ increases with the downstream distance of the panels. The level of $\tilde{p}$ on panel 1 (partially upstream of the nozzle exit) is reduced nearly an order of magnitude from the loading on panel 4. Since panel 4 is at a lower angle to the jet axis, this is in agreement with the directivity results in Fig. 7. The frequency spectra of the incident pressure are dominated by the fundamental frequency $f*$ and its harmonics. The relative harmonic content of the incident $\tilde{p}$ for panel 1 is significantly

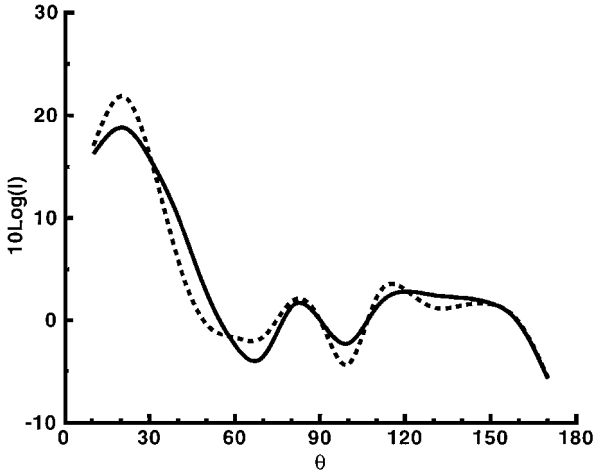

Fig. 7 Jet directivity of overall sound pressure level, with and without nearby structure: ——, with wall and - - - -, without wall.

increased as compared with the other (more downstream) panels, due to the preferred upstream beaming of high frequencies.

2. Panel Responses

The vibrating velocity v at the center of each panel is plotted in Fig. 9, together with the corresponding PSDs. The panels were held fixed until the leading pulse had passed. This eliminates any effect of the pulse in the panel responses but does lead to an impulsive start to the panel motion. For this reason, only the long-time responses of the panels are investigated. The panel responses increase with distance until they reach a maximum on panel 3 and then decrease slowly with distance. The relative subharmonic level is increased as compared with the incident pressure. This may be due to the receptivity of the panels to low-frequency excitation. The predominant responses of the panels, however, are at the jet fundamental frequency $f*$ and its harmonics. The relatively large harmonic contribution to the response of panel 1 is indicative of the preferred upstream beaming of high frequencies, although the overall response is smaller than that of the more downstream panels.

The observation made in Refs. 1 and 2 that the panels act as narrow filters, converting a broadband input into a narrow-band

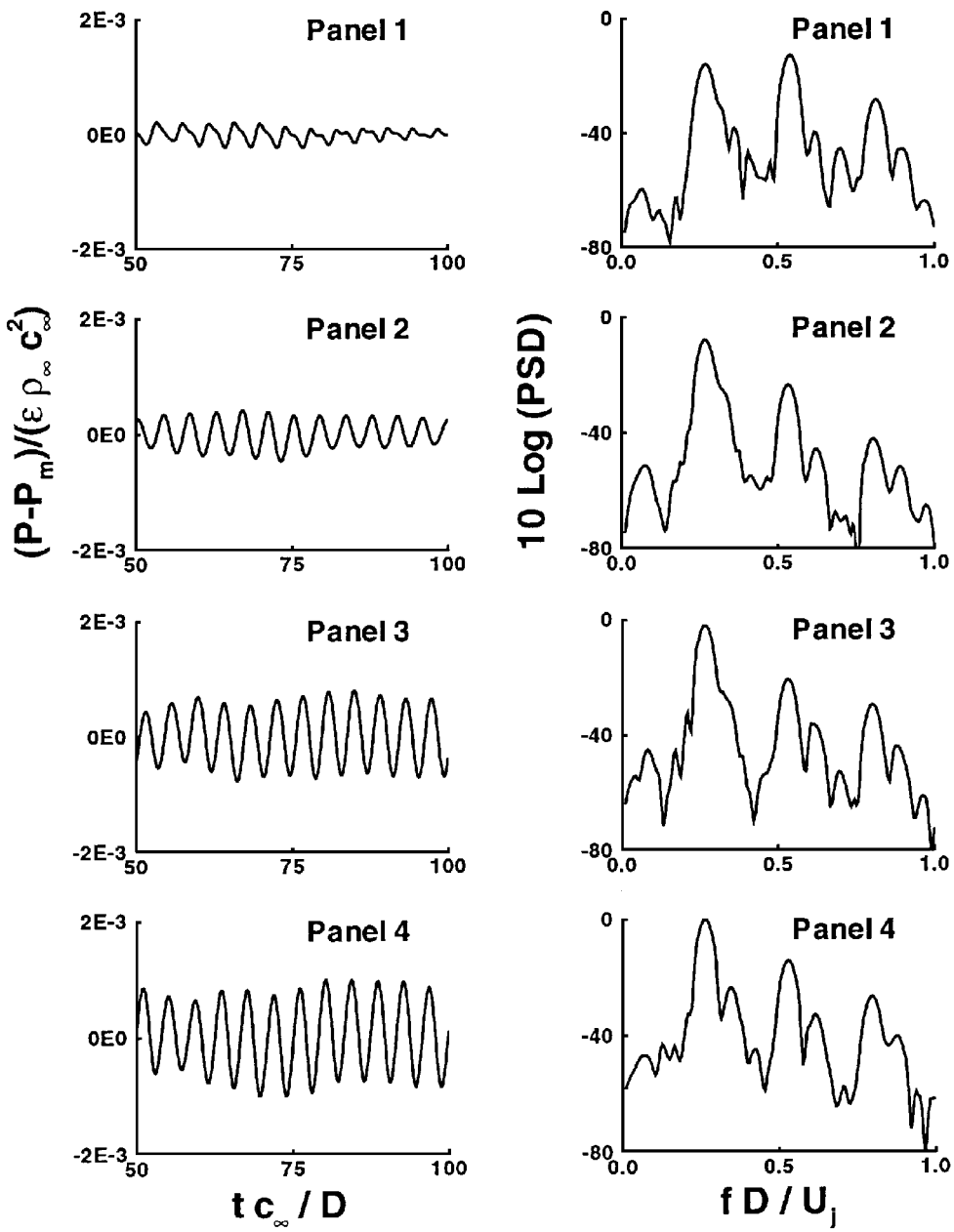

Fig. 8 Panel pressure loading time histories and spectra.

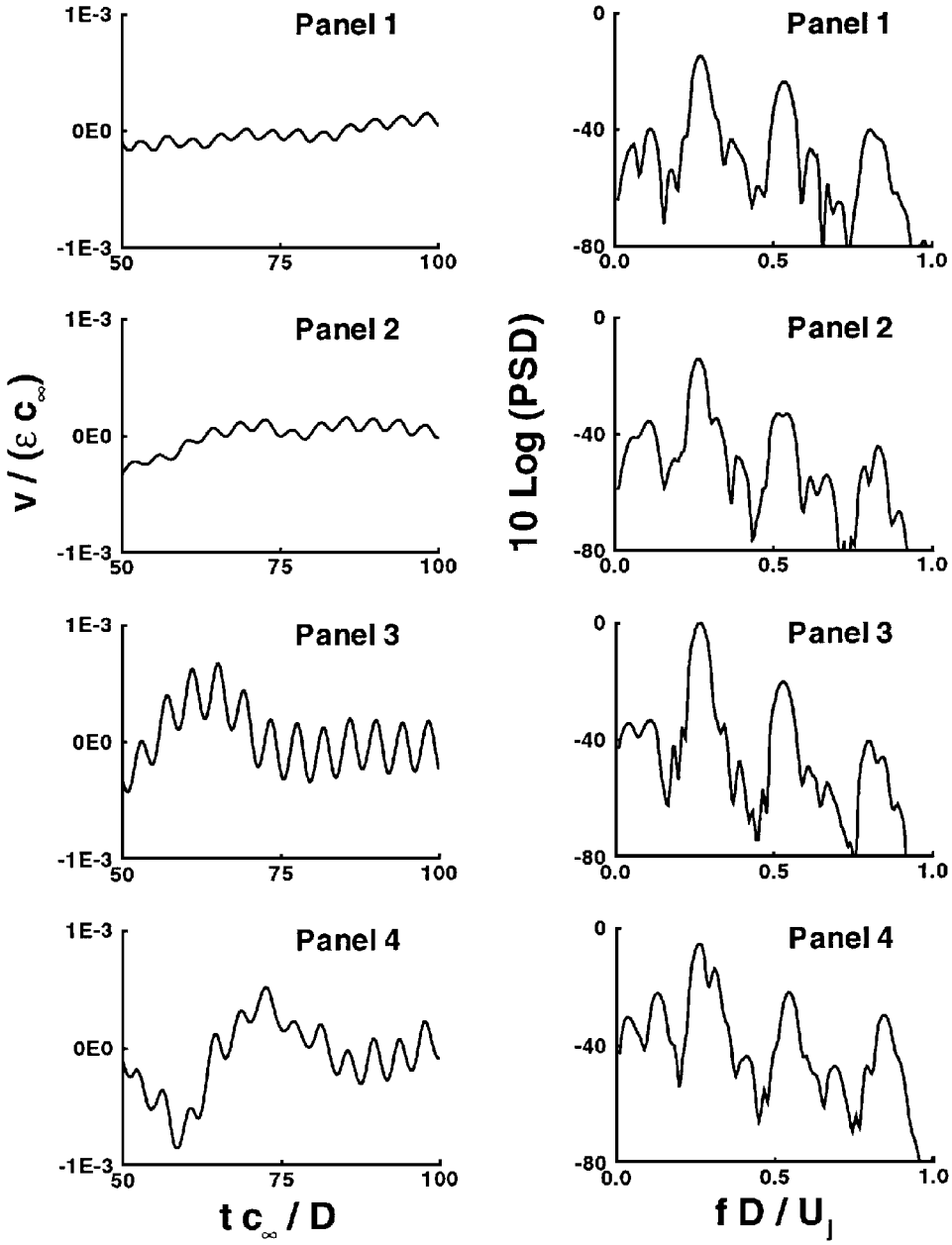

Fig. 9 Panel velocity time histories and spectra.

response may no longer be relevant for jets dominated by the long-time vortex shedding considered here. In this case the panels respond clearly at the frequencies of the loading, somewhat enhancing the subharmonic response.

3. Radiation Domain

The panel radiation is considered next. The pressure $\tilde{p}$ is computed along the line $y = 25D$ in the radiation domain. Shown in Fig. 10 are time histories and PSDs for four different x locations along this line. It can be seen that the overall level of radiation is reduced as x decreases, i.e., in the upstream direction in terms of the jet flowfield. The PSDs indicate that for downstream locations there is peak radiation at S_r*, the first two harmonics, and the subharmonic. For upstream locations, a low-level, relatively broadband spectrum is found. Thus the radiated sound is beamed primarily in vertical and downstream directions and is controlled by $f*$, i.e., the vortex shedding frequency of the jet.

In Fig. 11 the overall intensity is computed as a function of x. This figure illustrates the strong vertical and downstream beaming of the panel radiation. It also illustrates a zone of relative silence at about $x/D = 15$ where the intensity is reduced by about 15 dB from nearby locations. This zone can also be seen in the flowfield in Fig. 6 and is due to destructive interference between radiation from the various panels. No such zone was observed at lower jet Mach numbers,[1,2] where the resulting radiation was more heavily influenced by the starter pulse and the sound generated by the leading instability wave in the jet.

In a real jet, instabilities can be generated by bursts within the jet, generating large-scale structures, as simulated by the starter pulse and the intermediate time behavior of the jet. Also, instabilities can be generated in a more continual fashion via vortex shedding, as is done here, by considering the long-time evolution of the model. The model allows for a separation of these effects so that they can be studied separately.

C. Comparison with Lower Mach Number Jet

The results described earlier show that for the high subsonic Mach number jet the long-time jet response is concentrated in a relatively narrow band around $S_r* \simeq 0.25$ together with harmonics. The panel response and radiation exhibits a similar behavior. The mechanism dominating the jet/structure response is vortex shedding from the nozzle lip. Thus, for high subsonic Mach number jets, the primary effect of the panels is to transmit the vortex shedding response into the radiation domain.

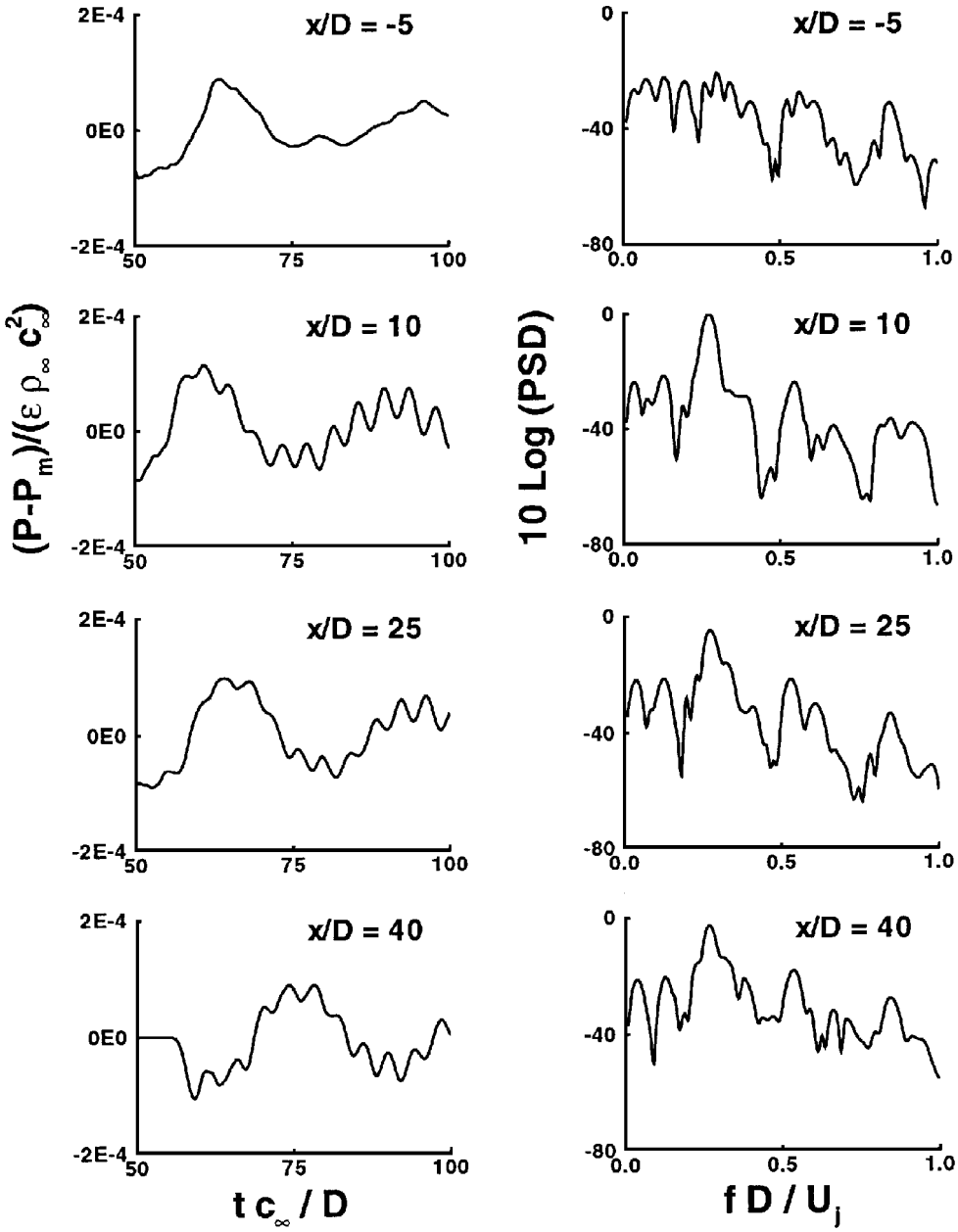

Fig. 10 Radiation domain far-field time histories and spectra at *x/D* = _5, 10, 25, and 40 along the line *y/D* = 25.

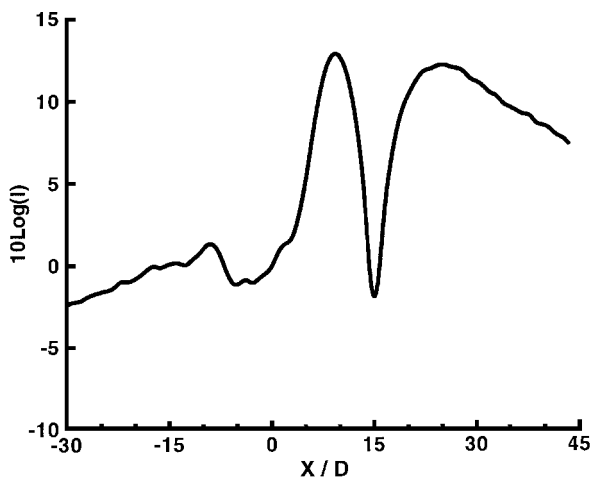

Fig. 11 Radiation domain directivity of overall sound pressure level along the line *y* = 25*D*.

An entirely different behavior occurs for lower Mach number jets. In this case, the effect of vortex shedding is considerably reduced. The jet response is concentrated in low frequencies and does not exhibit any pronounced spectral peaks. To illustrate this, the present results are compared with those of a jet at a Mach number of 0.65. This is the same Mach number considered in Ref. 1 (although longer times and a contracting nozzle are considered as described earlier).

In Fig. 12, the spectra for both the incident pressure and panel velocity at the center of panel 3 are plotted for both the high and low Mach number jets. The forced response of the panels at $M_j = 0.90$ is clear. The spectrum of the panel response is very similar to that of the panel loading, concentrated in bands around $S_r^* \simeq 0.25$, the shedding frequency, and harmonics. In contrast, the incident pressure for $M_j = 0.65$ shows no pronounced spectral peaks over a broad low-frequency range. In this case the panels act as narrow-band filters, converting this relatively broadband jet response into discrete spectral bands associated with the natural frequencies of the panels. The vortex shedding is much weaker, the long-time jet response is dominated by sound generated from the initial instability wave, and the overall sound from the jet is much reduced. The

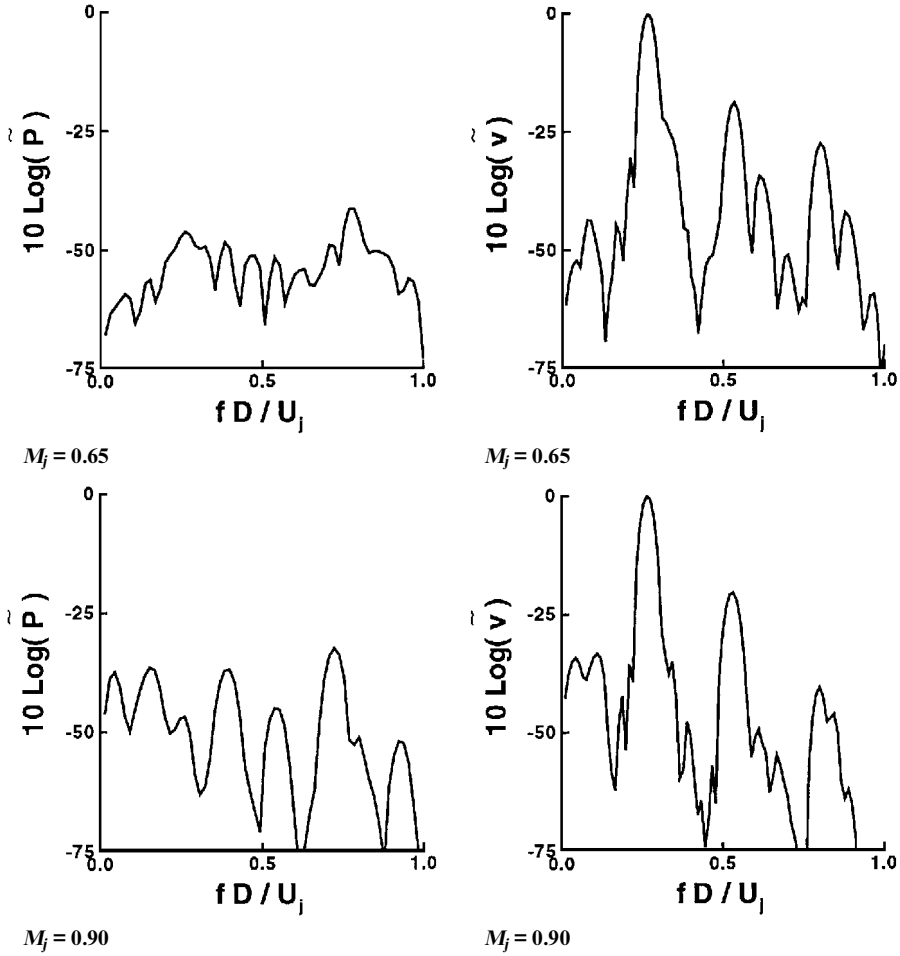

Fig. 12 Spectra for incident $\tilde{p}$ and v at center of panel 3 for $M_j = 0.90$ and 0.65.

far-field pressure in both the jet domain and the radiation domain exhibits similar behavior.

Thus, the results show a qualitatively different behavior as M_j is increased. For high subsonic Mach number jets the long-time behavior is dominated by vortex shedding. The panels act to transmit the vortex shedding frequencies to the radiation domain due to the forced response of the panels. For lower Mach numbers the vortex shedding is much weaker and the panels act to filter a broadband loading into relatively discrete low-frequency spectral bands.

IV. Conclusions

A numerical simulation has been conducted of a nearly sonic jet exhausting into a fluid at rest both with and without the presence of a nearby structure. The structure is rigid except for four flexible aircraft-type panels. These panels respond to acoustic forcing from the jet and radiate sound into both the jet domain and a domain on the other side of the panels. The simulation utilized a full coupling between the Euler equations (solved on either side of the panels) and the nonlinear beam equation, resulting in a full coupling between the flow, acoustics and panel response, and radiation. The results are in qualitative agreement with experimentally observed phenomena indicating the present model is capable of capturing the important features of jet flow/acoustic/structural interactions at nearly sonic jet exit velocities.

In particular, the results indicate the following properties of the long-time response of excited, high subsonic Mach number jets.

1) There is a nearly periodic shedding of vorticity from the nozzle lip. This shedding is associated with pressure disturbances that lead to far-field sound.

2) The shedding frequency scales with Strouhal number; S_r* is near 0.25, which is near the peak of many observed far-field radiation patterns.

3) The relative harmonic content of $\tilde{p}$ increases with upstream angle.

4) The far-field sound peaks near 30 deg.

All of the aforementioned are consistent with the features of previously observed real jets. Furthermore, the panel response and radiation results indicate the following.

1) The loading and response of the panels generally increase with downstream distance.

2) The frequency spectrum of the panel responses is dominated by the jet shedding frequency S_r*, its harmonics, and subharmonics.

3) The nature of the panel response is strongly dependent on the jet Mach number. For high subsonic Mach number jets, the panel response is forced at the shedding frequency and is very similar to that of the incident pressure. There is no discernible effect of the natural frequencies of the panels. Thus, the panels act to transmit the shedding frequency to the radiation domain. In contrast, for lower speed jets the panels act as narrow-band filters, converting the incident pressure, which shows no pronounced spectral peaks, into relatively discrete low-frequency bands that include both the natural frequencies of the panel and the jet instability waves.

4) The relative level of harmonics in the panel loading and response is increased for upstream panels.

5) Radiation is primarily in vertical and downstream directions.

6) The upstream radiation is small compared with downstream radiation and does not appear to reflect the jet shedding frequency.

7) Zones of relative silence occur due to destructive interference.

Finally, the code developed is computationally efficient, running at over 210 MFLOPS on a Cray Y-MP and over 550 MFLOPS on a Cray C-90. This produces a complete solution of the fully coupled flow/acoustic/structural interactions in approximately 6 CPU h (Cray Y-MP) on the relatively fine grids required to resolve these interaction phenomena.

Acknowledgments

The first author was supported by NASA Langley Research Center while in residence under a National Research Council Postdoctoral Research Associateship Award. The second author was partially supported by NASA Langley Research Center under Contracts NAS1-18605 and NAS1-19480 while in residence at the Institute for Computer Applications in Science and Engineering. Additional support was provided by National Science Foundation Grants DMS 93-01635 and DMS 95-30937. The authors thank J. C. Hardin for helpful discussions and comments.

References

[1]McGreevy, J. L., Bayliss, A., and Maestrello, L., "Interaction of Jet Noise with a Nearby Panel Assembly," *AIAA Journal*, Vol. 33, No. 4, 1995, pp. 577–585.

[2]Bayliss, A., Maestrello, L., McGrevy, J. L., and Fenno, C. C., "Forward Motion Effects on Jet Noise, Panel Vibration, and Radiation," *AIAA Journal*, Vol. 34, No. 6, 1996, pp. 1103–1110.

[3]Lighthill, M. J., "On Sound Generated Aerodynamically-I, General Theory," *Proceedings of the Royal Society*, Vol. A222, Ser. A, 1954, pp. 1–32.

[4]Lilley, G. M., "Theory of Turbulence Generated Jet Noise: Generation of Sound in a Mixing Region," U.S. Air Force, TR AFAPL-TR-72-53, IV, Wright–Patterson AFB, OH, 1972.

[5]Ribner, H. S., "Dryden Lecture, Perspectives on Jet Noise," *AIAA Journal*, Vol. 19, No. 12, 1981, pp. 1513–1526.

[6]Ribner, H. S., "An Extension of the Lighthill Theory of Jet Noise to Encompass Refraction and Shielding," NASA TM 110163, May 1995.

[7]Crow, S., and Champagne, F., "Orderly Structure in Jet Turbulence," *Journal of Fluid Mechanics*, Vol. 48, Aug. 1971, pp. 457–591.

[8]Kibens, V., "Discrete Noise Spectrum Generated by an Acoustically Excited Jet," *AIAA Journal*, Vol. 18, April 1980, pp. 434–441.

[9]Maestrello, L., Bayliss, A., and Turkel, E., "On the Interaction of a Sound Pulse with the Shear Layer of an Axisymmetric Jet," *Journal of Sound and Vibration*, Vol. 74, No. 2, 1981, pp. 281–301.

[10]Bechert, D. W., and Pfizenmaier, E., "On the Amplification of Broadband Jet Noise by Pure Tone Excitation," *Journal of Sound and Vibration*, Vol. 43, No. 3, 1975, pp. 581–587.

[11]Huerre, P., and Monkewitz, P. A., "Local and Global Instabilities in Spatially-Developing Flows," *Annual Review of Fluid Mechanics*, Vol. 22, 1990, pp. 473–537.

[12]Michalke, A., and Hermann, G., "On the Inviscid Instability of a Circular Jet with External Flow," *Journal of Fluid Mechanics*, Vol. 114, 1982; pp. 343–359.

[13]Michalke, A., "Survey on Jet Instability Theory," *Progress in Aerospace Science*, Vol. 21, No. 3, 1984, pp. 159–199.

[14]Bayliss, A., Maestrello, L., and Turkel, E., "On the Interaction of a Sound Pulse with the Shear Layer of an Axisymmetric Jet, III: Non-Linear Effects," *Journal of Sound and Vibration*, Vol. 107, No. 1, 1986, pp. 167–175.

[15]Maestrello, L., and Bayliss, A., "Flowfield and Far Field Acoustic Amplification Properties of Heated and Unheated Jets," *AIAA Journal*, Vol. 20, No. 11, 1982, pp. 1539–1546.

[16]Dowell, E. H., "Generalized Aerodynamic Forces on a Flexible Plate Undergoing Transient Motion in a Shear Flow," *Quarterly Applied Mathematics*, Vol. 24, No. 1, 1967, p. 331.

[17]Frendi, A., Maestrello, L., and Bayliss, A., "On the Coupling Between a Supersonic Boundary Layer and a Flexible Surface," *AIAA Journal*, Vol. 31, No. 4, 1993, pp. 708–713.

[18]Frendi, A., Maestrello, L., and Bayliss, A., "Coupling Between Plate Vibration and Acoustic Radiation," *Journal of Sound and Vibration*, Vol. 177, No. 2, 1994, pp. 207–226.

[19]Mankbadi, R., Hayder, M., and Povinelli, L., "The Structure of Supersonic Jet Flow and Its Radiated Sound," *AIAA Journal*, Vol. 32, No. 5, 1994, pp. 897–906.

[20]Maestrello, L., "Acoustic Energy Flow from Subsonic Jets and their Mean and Turbulent Flow Structure," Ph.D. Thesis, Inst. of Sound and Vibration, Univ. of Southampton, England, UK, 1975.

[21]Maestrello, L., and McDaid, E., "Acoustic Characteristics of a High-Subsonic Jet," *AIAA Journal*, Vol. 9, 1971, pp. 1066–1071.

[22]Macaraeg, M. G., Streett, C. L., and Hussaini, M. Y., "A Spectral Collocation Solution to the Compressible Stability Eigenvalue Problem," NASA TP 2858, Dec. 1988.

[23]Fenno, C. C., Streett, C. L., and Hassan, H. A., "Use of Finite Volume Schemes for Transition Simulation," *AIAA Journal*, Vol. 30, No. 4, 1992, pp. 1122–1125.

[24]Bayliss, A., and Turkel, E., "Radiation Boundary Conditions for Wave-Like Equations," *Communications on Pure and Applied Mathematics*, Vol. 33, 1980, pp. 707–725.

[25]Bayliss, A., and Turkel, E., "Far-Field Boundary Conditions for Compressible Flows," *Journal of Computational Physics*, Vol. 48, No. 2, 1982, pp. 182–199.

[26]Gottlieb, D., and Turkel, E., "Dissipative Two-Four Methods for Time-Dependent Problems," *Mathematics of Computation*, Vol. 30, No. 136, 1976, pp. 703–723.

[27]Zaman, K. B. M. Q., and Yu, J. C., "Power Spectral Density of Subsonic Jet Noise," *Journal of Sound and Vibration*, Vol. 98, No. 4, 1985, pp. 519–537.